Journal of the Mechanical Behavior of Biomedical Materials 93 (2019) 81–92

Contents lists available at ScienceDirect

Journal of the Mechanical Behavior of Biomedical Materials

journal homepage: www.elsevier.com/locate/jmbbm

Material anisotropy and elasticity of cortical and trabecular bone in the adult mouse femur via AFM indentation

Meisam Asgari[a], Jad Abi-Rafeh[b], Geoffrey N. Hendy[c], Damiano Pasini[a,*]

[a] Department of Mechanical Engineering, McGill University, 817 Sherbrooke Street West, Montreal, QC, Canada H3A 0C3
[b] Department of Medicine, McGill University, Montreal, QC, Canada H4A 3J1
[c] Metabolic Disorders and Complications, McGill University Health Centre Research Institute, Departments of Medicine, Physiology, and Human Genetics, McGill University, Montreal, QC, Canada H4A 3J1

ARTICLE INFO

Keywords:
AFM indentation
Elastic modulus
Cortical bone
Trabecular bone
Bone anisotropy
Bone heterogeneity
Bone viscoelasticity

ABSTRACT

This paper investigates the elastic properties of bone tissue in the adult mouse femur through Atomic Force Microscopy (AFM) indentation with the goal of understanding its microstructure and underlying mechanics at the nano length scale. Both trabecular and cortical bone types are studied. In particular, we examined the elasticity of cortical bone and individual trabeculae in the longitudinal and transverse directions of the samples. For cortical bone, the elastic modulus in the longitudinal direction was found to be 10–15% higher than that in the transverse direction; for trabecular bone, this difference was 42%. For the trabeculae, this value was found to be in a lower range (0.92 ± 0.22 GPa). As per the transverse elastic modulus, an average of 1.58 ± 0.36 GPa was measured for cortical bone, and 0.55 ± 0.21 GPa for trabecular bone. The anisotropy ratio was within the range of 1.2–1.5 for cortical bone and 1.7–2 for trabecular bone. While the elastic modulus of cortical bone varied along the length of the femur with up to 30% variation, no significant differences were observed within each transverse section. The effect of indentation frequency (1–500 Hz) on the longitudinal elastic moduli was also investigated for cortical and trabecular bone, with results showing a correlation between indentation frequency and elastic modulus.

Statement of significance: This study examines the adult mouse femur with a twofold aim: to investigate the anisotropy and inhomogeneity of cortical and trabecular bone tissues and to elucidate their elastic behavior at the nanometer length scale. The elastic moduli of cortical bone and individual trabecula are measured in the longitudinal and transverse cross-sections via AFM indentation at selected locations and in specific directions of the adult mouse femur. The results provide insights into the relationship between mechanical properties and structural morphology of cortical and trabecular bone tissue.

1. Introduction

Bone is a mineralized biological tissue with a complex hierarchical structure that is constantly remodeled throughout life. In addition to water, two main components comprise this biological tissue: a deformable organic phase and a stiff mineral phase. The former consists of approximately 90% collagen type I and 10% non-collagenous proteins; the latter is made of hydroxyapatite minerals. The composition and structural arrangement of the basic components play a key role in the capacity of bone to provide structural support, as well as in serving numerous vital functions such as the facilitation of locomotion, support of mastication, and protection of vital organs (Olszta et al., 2007; Lees, 1987; Hamed and Jasiuk, 2012; Martin et al., 2004).

The degree of anisotropy and heterogeneity of bone tissue is mainly governed by its basic constituents along with their composition and structural organization. In the skeleton of mammals, the three main components include organics, predominantly type I collagen (32–44%), minerals (33–43%), and water (15–25%). These constituents appear in both cortical and trabecular bone, the macrostructural organizations of bone tissue. Cortical bone is dense and solid, and predominantly surrounds the hollow marrow space of long bones at the diaphysis. At the nanoscale, its compact microstructure consists of cross-linked collagen monomers, water, and non-collagenous proteins, reinforced by hydroxyapatite-like nanocrystals that form mineralized collagen fibrils lying within an extra-fibrillar hydroxyapatite matrix (Lees, 1987; Garner et al., 2000; Sharir et al., 2008; Depalle et al., 2016; Fratzl et al., 2004; Buehler, 2006, 2007; Fratzl, 2008; Hamed et al., 2010). The result is a single lamella that contains lacunar cavities. There are several layers of

* Corresponding author.
E-mail address: damiano.pasini@mcgill.ca (D. Pasini).

https://doi.org/10.1016/j.jmbbm.2019.01.024
Received 27 September 2018; Received in revised form 28 January 2019; Accepted 30 January 2019
Available online 31 January 2019
1751-6161/ © 2019 Elsevier Ltd. All rights reserved.

lamellae arranged in concentric rings around the vascular channels forming osteons, whereas interstitial lamellae fill spaces between osteons (Hofmann et al., 2006; Rho et al., 1998; Weiner and Wagner, 1998; Gibson, 1985; Currey, 2002; Carter and Beaupre, 2007; Turner and Burr, 1993; Ashman and Rho, 1988; Rho et al., 1997; Weiner et al., 1999; Cowin, 2001; Reznikov et al., 2014). On the other hand, dissimilar to cortical bone is the microarchitecture of trabecular bone (Choi and Goldstein, 1992), a cellular solid comprised of a network of plates and rods with pores filled with bone marrow. While trabecular bone is morphologically comparable to cortical bone, its composite structure, which is arranged in packets of lamellar bone, comprising hydroxyapatite, collagen, and water, is weaker and easier to fracture (Reznikov et al., 2015; Keaveny et al., 2001; Choi and Goldstein, 1992). Besides porosity, trabecular bone differs from cortical bone for the presence of inclusions of unremodeled embryonic bone, and for the abundance of cement lines per unit volume. Whereas an osteon of 200 microns in diameter is all solid lamellar bone except for the central canal surrounded by one cement line, a single trabecula approximately shaped like a 200-micron diameter cylinder generally consists of a patchwork of tens of overlapping lamellar packets, separated from each other by multiple cement lines. Such lines are not only bone interfaces with distinct mechanical properties, but also the sites of docking for osteoclasts, i.e., the bone-resorbing cells (McKee and Nanci, 1996).

Understanding the mechanical properties of bone tissue has been the subject of intense research conducted for years through a diverse range of experimental investigations across the spectrum of length scale from nano to meso scale (Zysset et al., 1999; Donnelly, 2011). Elastic stiffness, viscoelasticity, fracture toughness, and other mechanical properties have been studied for both cortical and trabecular bone. Standard mechanical testing involving tension, compression, torsion, three-point bending, and buckling has been used to measure the macroscopic properties of bone tissue (Townsend et al., 1975; Ryan and Williams, 1989; Bayraktar et al., 2004; Beaupied et al., 2007; Woo et al., 1991). While these early studies and other similar ones have focused on the elastic bulk properties, they fall short in capturing the distinct morphological features of bone observed at the micro and nanoscale, thus being incapable of differentiating the elastic response of each structural constituent. For this purpose, ultrasound microscopy (Eriksen et al., 1994; Bala et al., 2013; Hengsberger et al., 2002) has been proposed as an alternative tool for investigating the local response of the bone tissue. While acoustic reflectivity can be successfully measured uniformly within each structural unit, and non-uniformly between structural units, the elastic modulus, which depends on relative density, cannot be assessed (Katz and Meunier, 1993). To address this limitation, nanoindentation has been often used to locally measure bone tissue properties. Compared to ultrasound microscopy, nanoindentation can discriminate between the elastic moduli of a living tissue at any given point within an area of a few micrometers (Hengsberger et al., 2002). Several investigations have been performed (Fan et al., 2006; Rho et al., 1993; Turner et al., 1999; Rho et al., 1999), with those by Rho et al. (1993), Rho et al. (1999), Rho and Pharr (1999), Thurner (2009), Zysset et al. (1999), Donnelly et al. (2006), Katsamenis et al. (2015) and Hengsberger et al. (2002) being among the most notable. For example, in the works of Zysset et al. (1999) and Rho and Pharr (1999) nanoindentation was used to characterize not only the microstructure and mechanical properties of cortical and trabecular bone in human and bovine femoral bone but also their level of hydration with respect to anatomical location and age. Furthermore, Rho et al. (1997) measured the elastic properties of the trabecular bone of human vertebrae and the cortical bone of human tibia. In addition, reference point indentation has been applied to conduct *in vivo* measurements of bone material properties (Hansma et al., 2006; Setters and Jasiuk, 2014; Idkaidek et al., 2017). Used for oddly-shaped materials or for materials coated by a softer material, this technique is unique as it establishes a relative reference point at the location of indentation. Besides nanoindentation, Atomic force microscopy (AFM) is another powerful alternative to capture topographical information and elastic properties of materials at the micro and nanoscale, as shown by its extensive application to biomaterials (Fig. 1). One main advantage of AFM indentation over other micro-mechanical testing techniques is that the local deformations may be set to remain purely elastic with no permanent deformation on the sample and that the indentation area can be accurately selected. Applied to bone tissue, AFM indentation reveals morphological characteristics defining local properties and anisotropy at the microscale. It also enables to focus on relatively homogeneous regions while disregarding others containing pores and local defects (as small in radius as 15 nanometers), which are typical of bone tissue.

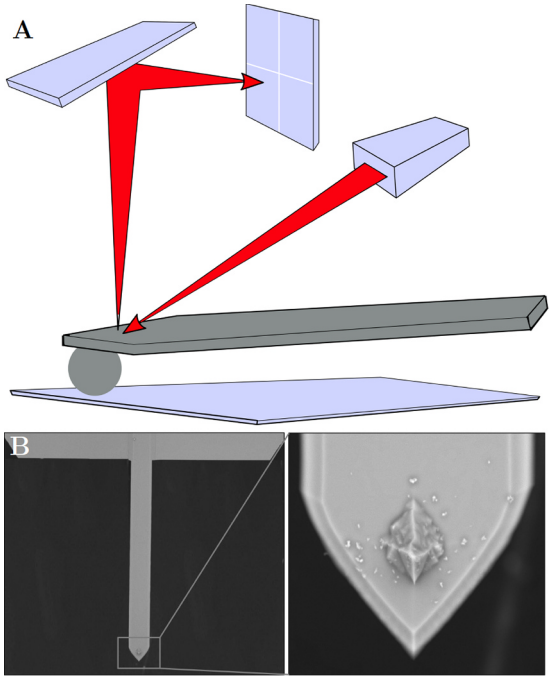

Fig. 1. Brief description and principle of operation of AFM technology. AFM is a type of scanning probe microscopy that does not rely on lenses or beam irradiation to obtain sample images and force measurements. Because it does not suffer from spatial resolution caused by diffraction and aberration, it can attain resolution of about 1000 higher than that offered by classical optical imaging systems. These characteristics are commonly exploited to study materials at the micro and nano length scale. AFM is used to both image and test material samples to obtain topographical information, elastic stiffness, and electrical conductivity among other properties. A: The technology comprises a sharp tip with radius of the order 2–100 nm mounted on a 50 to 150 μ m cantilever that scans the sample surface, thus providing access to its nanoscale topography. As the tip enters into contact with the sample, the interaction between the tip and the surface makes the cantilever deflect, and this deflection is measured through a laser beam by a detector. During the contact, the deflection of the cantilever, which correlates with the surface topography of the sample, is translated into an image. Besides imaging, AFM can measure the local elastic modulus of materials by pushing a spherical tip mounted on the cantilever into the surface of the sample. B: Transmission Electron Microscopy (TEM) images of an AFM cantilever with a spherical tip.

Despite the advantages of AFM indentation, a paucity of work exists in the literature that investigates the directional as well as the time-dependent response of bone tissue at the micro and nano length scale in both cortical and trabecular bone (Wallace, 2012; Thurner, 2009; Hassenkam et al., 2004). This work is the first investigation using AFM indentation on the mouse femur. A systematic nanoscale assessment is carried out on the anisotropy and inhomogeneity of its cortical and trabecular bone tissue. In particular, we shed light on the nanoscale elastic response of cortical bone specimen and individual trabeculae with measures that differ from bulk properties typically obtained through macro-scale experiments. The results can gauge the level of

inhomogeneity and anisotropy of bone tissue across representative longitudinal and transverse cross-sections of the femur as well as quantify the directional changes of the elastic moduli. Another novel aspect of this work is the nanoscale assessment of the frequency-dependent elasticity of both cortical and trabecular bone tissue at representative loading rates.

2. Materials and methods

2.1. Mouse femora and sample preparation

Three femora were harvested from three male mice of nine months of age. Men1flox/flox mice were obtained from The Jackson Laboratory (129S(FVB)-Men1tm1.2Ctre/J) (Crabtree et al., 2001) and were phenotypically indistinguishable from wild-type mice (Crabtree et al., 2001; Kanazawa et al., 2015). The average weight of the mice was 35.64 g (n = 3: 33.95, 37.26, 35.71), a value consistent with previous data (36.51 g (n = 10)) for mice of the same sex, age and strain (Kanazawa et al., 2015). Mice were maintained on a mixed FVB and C57BL/6J background in a pathogen-free standard animal facility, and experimental procedures were performed following an animal use protocol approved by the Animal Care and Use Committee of McGill University in accordance with Canadian Council on Animal Care guidelines. Femoral bone samples were first dissected and embedded in Methylmethacrylate. Longitudinal and transverse sections of 50–100 μ m thickness were then cut using a microtome (Leica RM 2165) with a diamond blade for AFM (similar to the method by Xu et al. (2003)). The cut sections were then placed in three changes of 2-methoxyethylacetate for 20 minutes each, two changes of acetone for 5 minutes each, and two changes of deionized water for 5 min each, to separate Methylmethacrylate. Sections were fixed on microscope slides. The surface of the cut sections was slightly polished using a polishing cloth (Anamet, Montreal, QC, Canada) prior to indentation tests to minimize residual surface roughness.

2.2. Atomic force microscopy

A JPK Atomic Force Microscope (JPK Nano-wizard@3 BioScience, Berlin, Germany) was used for imaging and force spectroscopy. The maximum lateral scan focused on regions of area 30 μ m × 30 μ m, and AFM images were obtained at a resolution of 1024 × 1024 pixels. Indentation force measurements were made at representative points on the longitudinal and transverse sections. The longitudinal elastic modulus E_l refers to the transverse cross-section perpendicular to the femur axis, and the transverse elastic modulus E_t refers to a measurement taken along a longitudinal cross-section parallel to the axis of the femur. The majority of the measurements were performed in the dry state and others with samples immersed in 1x Phosphate Buffered Saline solution (1x PBS containing 137 mM NaCl, 2.7 mM KCl, 8 mM Na_2HPO_4, and 2 mM KH_2PO_4). Using the force module of the JPK AFM, a force map was created within an area of 30 μ m × 30 μ m of each sample. Non-conductive silicon nitride cantilevers (MLCT Microcantilever, Bruker, Mannheim, Germany) with integrated spherical tips of radius 2 nm, and super-sharp standard Force Modulation Mode Reflex Coating (FMR) cantilevers (Nanotools USA LLC, Henderson, NV) with diamond-like carbon nano-tip (radius 2–3 nm, nominal resonance frequency 75 kHz, and length 225 μ m) were used for contact mode imaging. Non-Contact High Resonance (NCHR) cantilevers (Nanotools USA LLC, Henderson, NV) [nominal spring constant 40 N/m, integrated spherical tips of radii 50 nm (± 10%), 100 nm (± 10%), and 300 nm (± 10%), nominal resonance frequency 330 kHz, and length 125 μ m] were used for indentation measurements. The indentation frequency was selected in the range 1–500 Hz. The deflection sensitivity of the piezo module was established by probing the surface of the glass substrate. A thermal tuning method was then used to calibrate the stiffness of the cantilever.

Repeat indentations were made at given locations for consistency and to ensure that no permanent deformation occurred at the surface of the sample. Force maps containing 64 × 64, 128 × 128, or 256 × 256 indentation points (depending on the indentation frequency) were created on each indentation area. The AFM probes with the radii of 50, 100, and 300 nm were selected for indentation. The elastic modulus E of a sample was obtained through Hertzian contact mechanics, where $E = 3F(1-\nu^2)/4\sqrt{R\delta^3}$ is the relation between the elastic modulus E and the applied indenting load F with ν being the Poisson's ratio of the sample, R the radius of the spherical probe, and δ the indentation depth. A number of assumptions were considered. The deformation of the sample relative to its thickness and also relative to the radius of the probe was assumed very small. Any strain below the elastic limit was also assumed infinitesimal, a condition satisfied with the use of an indentation depth below 50 nm that rules out the influence of the glass substrate as well as any nonlinear and inelastic behavior of bone at higher strains. The Poisson's ratio ν was within the range of 0.2–0.45. Data analysis was performed with the JPK data processing software.

2.3. Statistical analysis

Sections from three femoral bone samples of three mice of identical age (9 months) were tested, with data here reported as mean value and standard deviation (SD). One-way analysis of variance was used to discriminate any differences among means of groups of data. Paired Student's t-test was also used to assess differences between two sets of individual data. Differences were considered significant at $p < 0.05$.

3. Results

3.1. AFM images of the microstructure of cortical and trabecular bone

Fig. 2A shows AFM images of areas in selected transverse sections of femoral cortical bone; Fig. 2B visualizes the microstructure of trabecular bone with pores in a longitudinal section. The images show collagen fibrils within bone tissue that are coated with minerals (Hansma et al., 2005). Cortical bone has a monolithic structure with low porosity, whereas trabecular bone contains relatively large pores on the order of micrometers. Several grain structures appear with close packing. Mineral plates can still be observed on the surface of the trabeculae as a result of the sample preparation striven to be minimally disruptive.

3.2. Representative AFM indentation results

The indentation test was conducted on samples from both cortical and trabecular bone (Fig. 3), with curves in Fig. 3A_1 and Fig. 3B_1 showing their respective indentation forces. Each curve illustrates the interaction between the AFM probe and the bone tissue as the probe is pushed on the sample surface up to a certain indentation depth; the area within their loading and unloading paths denotes the dissipation energy. To minimize the deformation of the sample and the influence of the glass substrate, the samples were indented with low magnitude forces, below 400 nN for cortical bone, and 200 nN for trabecular bone. The elastic modulus of a sample was estimated from the curve of the force-indentation depth via a Hertzian contact model. The indentation depth was chosen in our experiments to be much smaller than both the thickness of the sample (100 μm) and the radius of the indenting sphere (50–300 nm). On one hand, the use of a very low indentation depth (≤ 5 nm) was avoided to minimize the signal-to-noise ratio during the experiments. On the other hand, a large indentation depth (≥ 200 nm) that might capture the influence of the underlying glass substrate was not pursued. As described in the method section, the results were obtained with an indentation depth below 50 nm to exclude nonlinear and substrate effects, as well as large elastic and plastic deformations. These

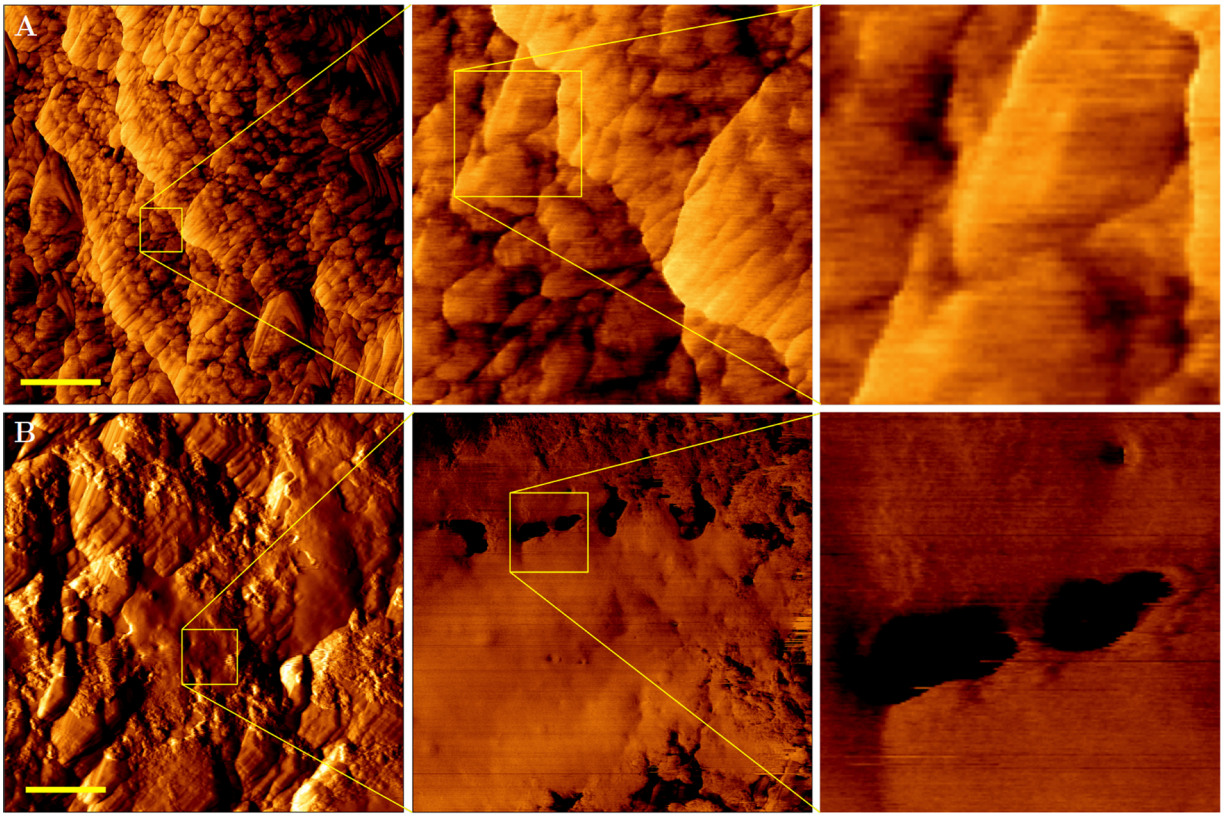

Fig. 2. Representative AFM images of cortical and trabecular bone types within a mouse femur. Each image shows porosity within their microstructure. A: Image of areas within cortical bone in a transverse section; B: Image of the microstructure of trabecular bone in a longitudinal section. All images were obtained in contact mode at 1 Hz line frequency. The scale bars represent 2 μ m.

conditions are enforced to satisfy one main AFM requirement, which prescribes a very low ratio of the indentation depth to the specimen thickness. An increase in the indentation depth might yield higher values of the elastic modulus, but this could cause permanent deformation, a condition that we persistently strived to avoid. As a result our values express purely elastic deformations with no permanent damage.

Fig. 3A_2 plots the distribution of data versus the elastic modulus in an area within the cortical bone of the femur diaphysis in the transverse section. The red rectangles represent the experimental measures, and the solid blue curve is the Gaussian curve of the best fit. Fig. 3B_2 pertains to the trabecular bone in the longitudinal direction. Fig. 3A_3 shows a representative force map for cortical bone without pores; 128 × 128 indentation points (yellow dots) were tested in an area of 10 μm × 10 μm of a monolithic transverse section. Analogously for trabecular bone, Fig. 3B_3 shows the respective force map with indentation points in an area of 5 μm × 5 μm across a longitudinal cross-section. Also here, pores of any size were excluded from indentation. For a given indentation depth on any transverse section, the maximum force measured on the cortical bone (~ 350 nN) was above the value obtained for trabecular bone (~ 150 nN), thereby indicating higher stiffness.

In the middle cross-section of the cortical region (Fig. 3A), the elastic modulus reached a maximum of 1.27 ± 0.41 GPa, a value obtained from the Gaussian regression functions of the indentation analysis at 1 Hz indentation frequency. At the loading rate of 500 Hz, however, the elastic modulus ranged from ~ 1.5–2.5 GPa with a peak at 1.57 ± 0.86 GPa, hence showing a correlation between stiffness and indentation frequency. A similar dependence was also observed for trabecular bone (Fig. 3B). At the indentation frequency of 1 Hz, the maximum elastic modulus at the femoral head was 0.74 ± 0.14 GPa, a value that increased to 0.92 ± 0.15 GPa at higher frequencies. Statistically significant differences were found between the elastic moduli at 1 and 500 Hz ($p = 0.012$).

Fig. 4 shows the longitudinal variability of the transverse elastic modulus along selected sections of cortical bone. Both the longitudinal (E_l) and transverse (E_t) elastic moduli were measured on a set of regions across dry mouse femora. The former showed a maximum value of ~ 1.98 ± 0.62 GPa and a minimum value of ~ 1.70 ± 0.32 GPa for the cortical region. For the trabeculae, values of E_l were lower (~ 0.92 ± 0.22 GPa). As per the latter, i.e. E_t, an average modulus of ~ 1.58 ± 0.36 GPa was measured for cortical bone and ~ 0.55 ± 0.21 GPa for trabecular bone (Fig. 4).

Differences in the elastic measures along the longitudinal and transverse sections of our samples confirmed a high level of local anisotropy in both the trabecular and cortical bone. Compared to the elastic moduli measured in the transverse direction, a 20 to 30% increase was observed in the longitudinal direction (i.e., normal to the transverse cross-sections). Furthermore, the elastic moduli were ≈ 35–50% greater for the cortical bone than for the trabeculae, with the lowest elastic modulus being that of trabecular bone in the transverse direction. Table 1 shows the values of $\eta = E_l/E_t$ assessing the elastic anisotropy of trabecular and cortical bone.

Longitudinal elastic modulus of cortical and trabecular bones varies significantly with the given values of the Poisson's ratio. Fig. 5 shows E_l of cortical bone at the mid-diaphysis, and that of trabecular bone in the femoral head. For the former, E_l varied within the range of 0.48–1.16 GPa, whereas for the latter within 1.25–2.25 GPa. These values were obtained for the Poisson's ratio in the range 0.2–0.45 at the indentation frequency of 50 Hz, thereby showing a dependence of E_l to the Poisson's ratio for both bone tissues.

Fig. 6 shows the polar map of E_l across a transverse cross-section at the diaphysis region of a femur. The data within the cross-section

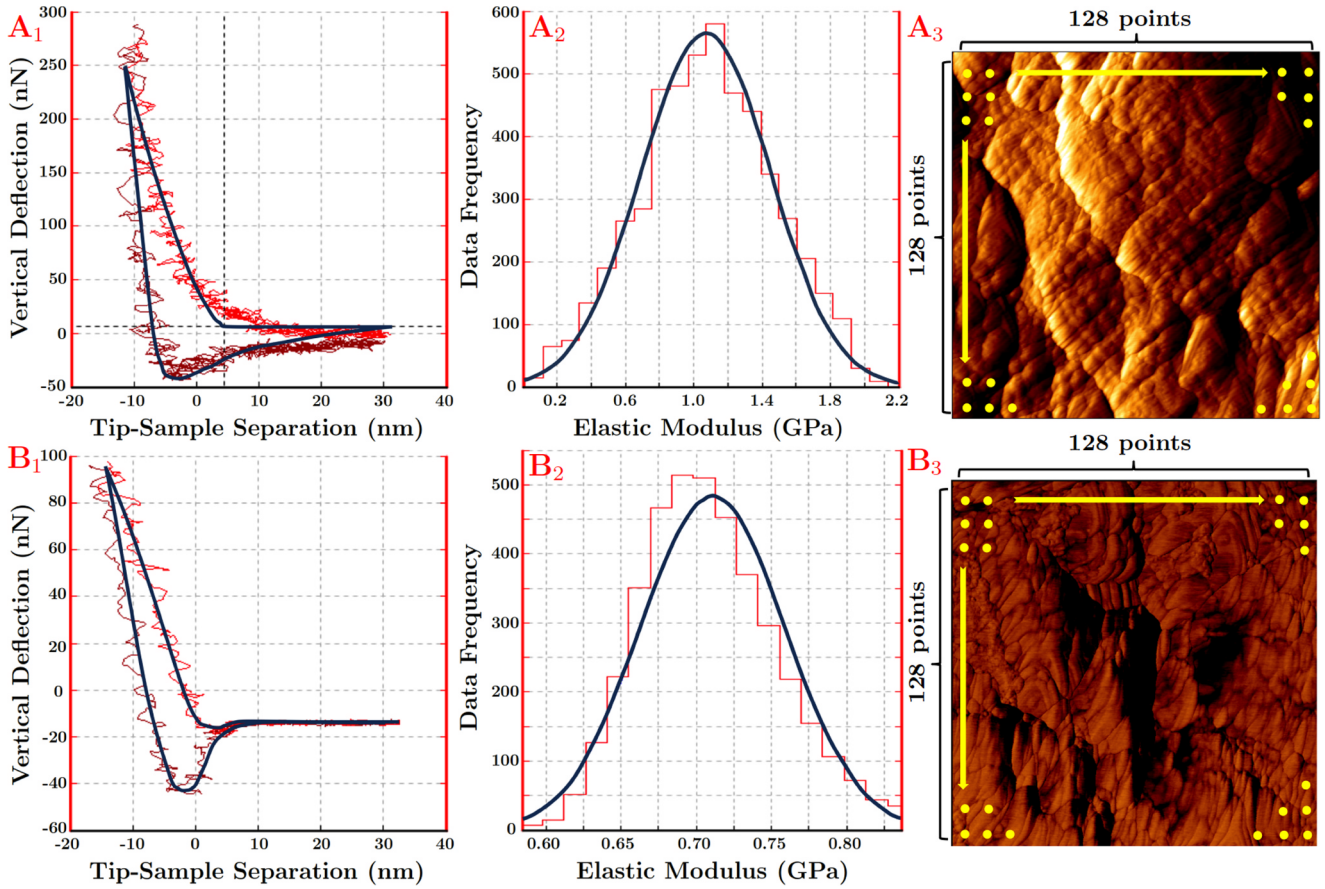

Fig. 3. Representative AFM indentation results; A_1: AFM indentation force plotted against the tip-sample separation for a point in the cortex of the femur diaphysis within a transverse section. The approaching curve and that representing retraction from the sample are shown; A_2: Plot of data distribution versus elastic modulus in an area within the cortex of the femur diaphysis in the transverse section. The red rectangles represent the experimental data and solid blue curve the Gaussian curve of best fit. The elastic modulus reached a maximum of 1.27 ± 0.41 GPa at the loading rate of 10 Hz; A_3: A representative force map including 128×128 indentation points in an area of $10\,\mu m \times 10\,\mu m$ of a monolithic transverse section of cortical bone that excludes pores. B_1: AFM indentation force plotted against the tip-sample separation for a point in the trabecular bone of the femoral head within a longitudinal section; B_2: Plot of the data distribution versus the elastic modulus for trabecular bone in the longitudinal direction; B_3: AFM height image of a force map including selected positions for indentation in an area of $5\,\mu m \times 5\,\mu m$ on a longitudinal section of trabecular bone. The indentation measurements at the loading rate of 10 Hz gave elastic moduli ranging from 0.60–0.87 GPa with a peak of 0.735 ± 0.140 GPa. At the same indentation depth, the maximum indentation load at cortical bone (~ 350 nN) was found to be greater than at trabecular bone (~ 150 nN) in transverse sections.

represent indentation points at 24 locations, each spaced at a similar angular distance. A, B, and C are bright and dark appearances of thick and thin microstructures. The variation of E_l within the transverse sections is almost negligible in the cortical region, and minor changes in E_l can be observed within each section.

Fig. 7 shows E_l variation of cortical bone along the transverse sections of the mouse femur, a result that parallels previous studies on human and bovine femora (Nobakhti et al., 2017; Wirtz et al., 2000). The morphological characteristics in both cortical and trabecular bone indicate a higher degree of inhomogeneity throughout the femur. As per the elastic moduli, lower values were measured at the distal regions of the femur, where the density of compact bone is lower than in the middle cross-sections. The measures show higher rigidity at the distal and proximal ends of the femur relative to the diaphyseal portion.

Fig. 8 shows a comparison of E_l and E_t of cortical and trabecular bone for three femur samples. E_l is above E_t, and both elastic moduli are higher in cortical bone than in trabecular bone. The highest value of the longitudinal elastic moduli measured in the transverse sections is aligned with the results of previous studies (Reilly et al., 1974). In terms of anisotropy, while a previous investigation on human cortical bone reported 15–25 GPa for the value of E_l (Rho et al., 1997), about two times E_t, our study on the mouse femur attests an anisotropy ratio of 1.2–2.

To investigate the effect of the AFM tip radius on the measured elastic moduli, a range of tip radii were tested. For larger size, the maximum force of indentation was increased to a level that could maintain the indentation depth constant. This choice led to consistent results indicating negligible changes in the measures of the elastic moduli.

Repeated measurements were also performed in the mid-diaphysis area of three cortical bone samples immersed in Phosphate Buffered Saline (PBS) solution. The results showed up to 22% decrease for E_l (~ 1.47 ± 0.21 GPa) and up to 27.5% decrease for E_t (~ 1.11 ± 0.24 GPa) due to sample hydration.

3.3. Frequency-dependent elastic behavior of trabecular and cortical bone

To investigate the loading rate dependency of the elastic behavior of trabecular and cortical bone samples, additional indentation tests were performed at given indentation frequencies from 1 to 500 Hz (Asgari, 2017). Fig. 9 plots the mean and standard deviation of the measured elastic modulus E of bone samples for given indentation rate $1/(T_e + T_r)$, where T_e is the extending time and T_r the retracting time of the probe during indentation, which were set equal at each loading rate (Asgari, 2017). In particular, Fig. 9A_1 illustrates E_l of cortical bone and Fig. 9B_1 shows E_l of trabecular bone, both measured at indentation frequency

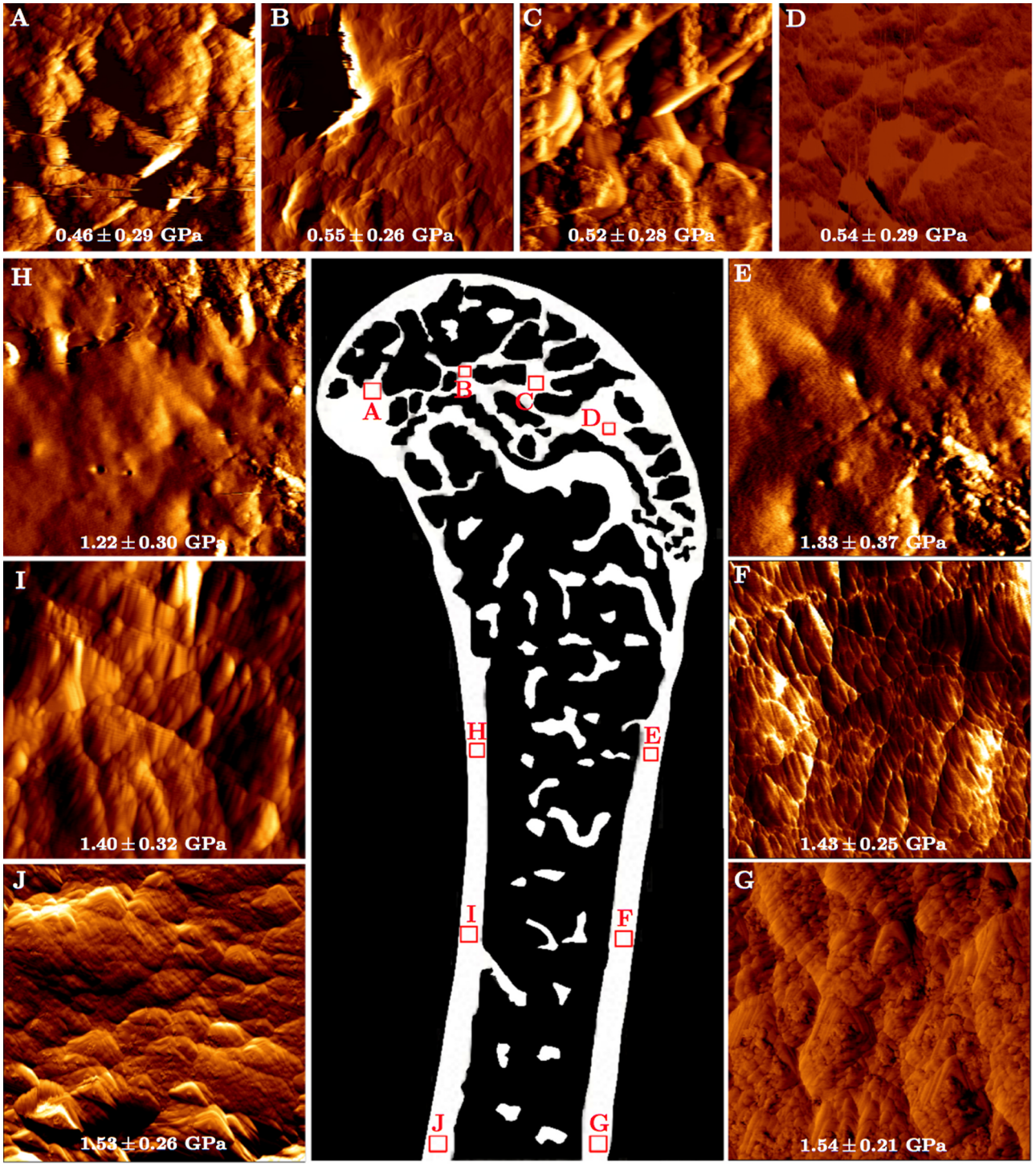

Fig. 4. Gradient linear elasticity map in a proximal half femur measured through indentation of longitudinal sections. The transverse elastic modulus E_t increases at the diaphysis of the femur. In areas of trabecular bone, the porosity in the bone microstructure becomes more obvious. Cortical bone has a compact microstructure with less porosity. The surface of the trabecular bone of mouse femoral head exhibits greater porosity and a lower elastic modulus than cortical bone.

Table 1
Elastic properties of various bone regions within a single femur in a dry state with the Poisson's ratio 0.3.

Bone type & localization	Elastic modulus E_l (GPa)	Elastic modulus E_t (GPa)	Anisotropy ratio $\eta = E_l/E_t$	Indentation points
cortical (metaphysis)	1.64 ± 0.31	1.33 ± 0.37	1.23	16378
cortical (mid-diaphysis)	1.90 ± 0.31	1.54 ± 0.21	1.23	16235
trabeculae (femoral head)	0.93 ± 0.20	0.54 ± 0.29	1.74	4035
trabeculae (distal epiphysis)	0.83 ± 0.31	0.47 ± 0.18	1.75	3631
trabeculae (metaphysis)	0.84 ± 0.29	0.43 ± 0.15	1.95	4014

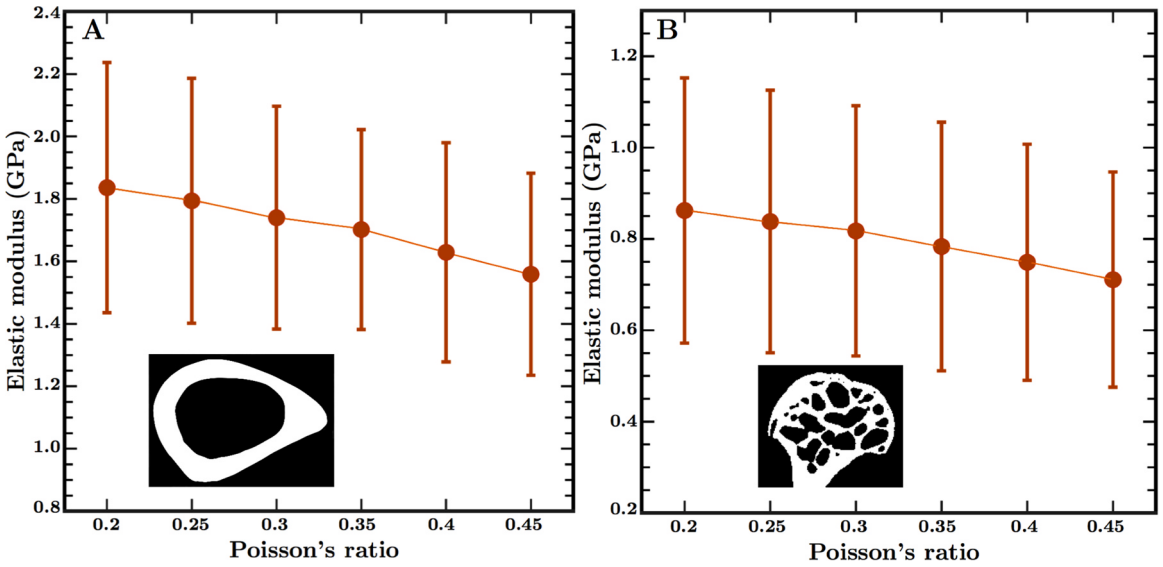

Fig. 5. A & B: Longitudinal elastic modulus E_l of cortical bone (mid-diaphysis) and trabecular bone (femoral head) for selected values of Poisson's ratio, ν (within the range 0.2–0.45), obtained by AFM indentation. Extend time T_e and retract time T_r are set to 10 ms. At given values of Poisson's ratio ν, the longitudinal modulus E_l of femoral head trabecular bone varies from 0.48–1.16 GPa, whereas the corresponding values for diaphysial cortical bone varies from 1.25–2.25 GPa.

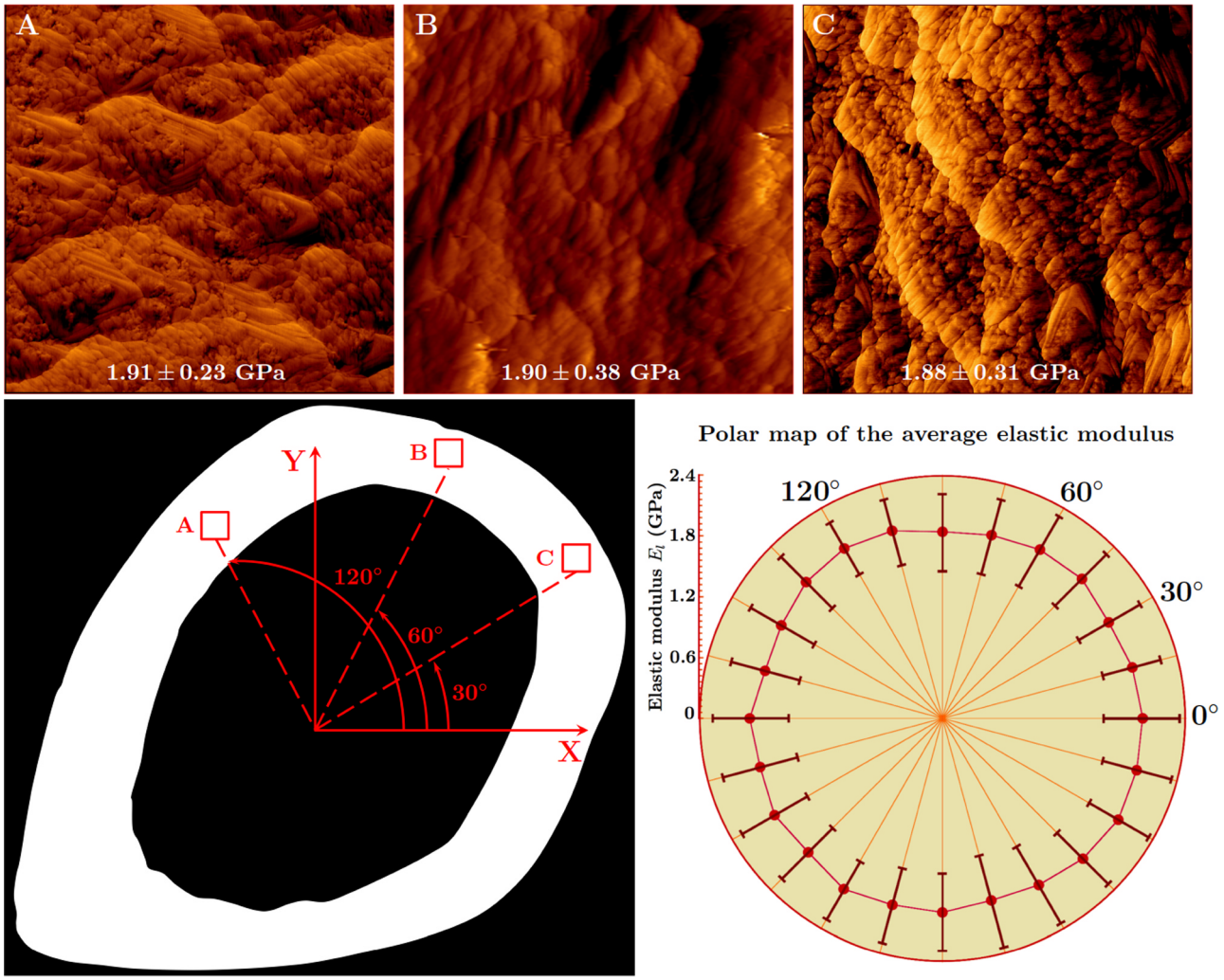

Fig. 6. Polar map of the elastic modulus E_l of cortical bone measured via AFM indentation, within a single transverse section in the diaphysis. The bright and dark appearances of thick and thin microstructures is observed within the AFM images of indentation areas. Twenty-four locations with a similar angular distance were selected within the cross-section for indentation. Selected sections in the middle of three femurs were tested, one of which is shown above. The polar map indicates only slight changes in the longitudinal elastic modulus of cortical bone within the single transverse section, and these changes are not statistically significant.

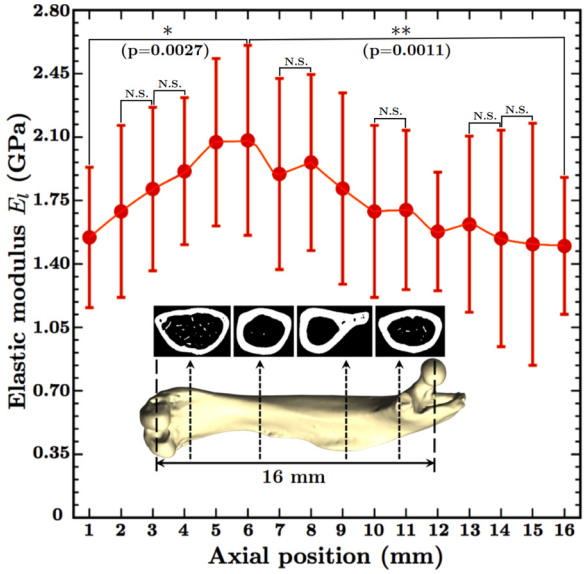

Fig. 7. Variation of the longitudinal elastic modulus E_l for cortical bone within transverse sections along the femur (distal metaphysis, distal diaphysis, proximal diaphysis and proximal metaphysis), measured via AFM indentation. The cortical bone longitudinal elastic modulus is less at the distal and proximal end of the bone relative to the diaphyseal portion. Significant differences are marked by * (p = 0.0027) and ** (p = 0.0011). N.S. represents no significant difference (p > 0.05).

from 1 to 500 Hz. Fig. 9A_2 and B_2 show, respectively, E_l of cortical and trabecular bone at 1–100 Hz plotted with a logarithmic fit. The elastic moduli of cortical and trabecular bone at higher frequencies were above those obtained at lower frequencies. Statistically significant differences were found between the elastic moduli at 1 and 500 Hz ($p < 0.05$). Fig. 9A_3 and B_3 depict the maximum indenting force in cortical and trabecular bone. For given values of the indentation depth, δ, below 50 nm, the indenting force, F, increased with the loading rate, showing the dependence of bone stiffness on loading rate. Furthermore, for a given indentation force, the indentation depth decreased with the loading frequency from 1 to 500 Hz. The large standard deviations of our experimental data, in particular at high frequencies, can be attributed to tissue heterogeneity, which varies with position in cortical and trabecular bone.

4. Discussion

4.1. Comparison of cortical and trabecular bone using AFM

The heterogeneous and anisotropic nature of both cortical and trabecular bone has been investigated through a range of techniques, such as atomic force microscopy imaging and indentation, nanoindentation, micro-tensile, and ultrasound testing. From the literature emerges a large variability of elastic moduli (Hassenkam et al., 2004; Swadener et al., 2001; Swadener and Pharr, 2001; Xu et al., 2003; Wallace, 2012; Thurner et al., 2007; Eppell et al., 2001; Thompson et al., 2001; Hansma et al., 2005; Kindt et al., 2005). For example, in a study on human vertebrae, the elastic moduli in the longitudinal direction of both trabecular and cortical bone were found significantly larger than those in the transverse direction (Rho et al., 1999). In another study on cortical tissue of human femur, a range of ~ 11.4–19.7 GPa was reported for the longitudinal elastic modulus, and a value of 10 GPa for the transverse elastic modulus, which results in an anisotropy ratio of ~ 1.45–1.75 (Reilly et al., 1974). Considering the individual trabeculae, the collective range of elastic modulus found in the literature is lower than that for cortical bone (Choi et al., 1990). This observation is generally attributed to the specific structural characteristics of a given bone type, its level of mineralization, and/or the orientation of collagen fibrils within the tissues, besides the location and orientations of the tested sample (Rho et al., 1993; Martin, 1991).

Besides structural characteristics, a number of non-mechanical factors such as sex, age, diet, medications, and physical exercise govern bone elastic properties. The dependence of cortical bone elastic properties on these factors was assessed in the young and mature bovine femur (Manilay et al., 2013). Through the use of optical microscopy and compression testing, previous works showed a direct dependence of stiffness and strength on the age of untreated bone, a reverse correlation between porosity content and bone tissue age, and the role of mineralization in mature bone (Manilay et al., 2013). The data reported in this work represent the nanoscale elastic moduli of mice of 9 months age at given directions and locations. A variability of the longitudinal elastic modulus (~ 30–35%) and transverse elastic modulus (~ 70%) appears along the femur, an outcome that may be attributed to mouse

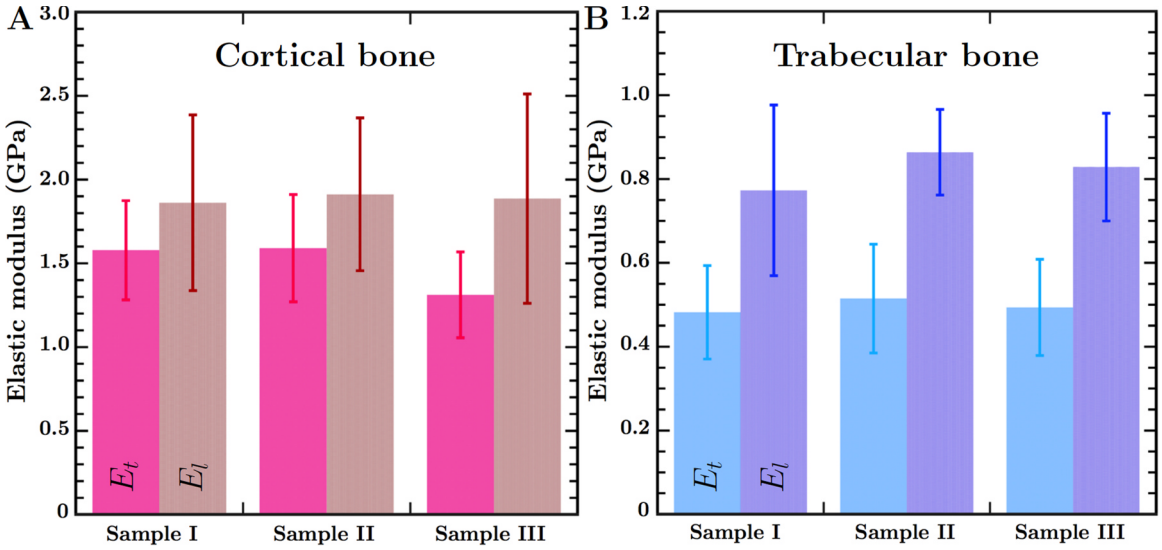

Fig. 8. A: Comparison of cortical bone transverse (left) and longitudinal (right) elastic moduli, E_t and E_l, of femoral bone samples from three mice; B: Counterpart comparison for the elastic moduli of trabecular bone. Statistically significant differences were found between the mean values of E_t and E_l in cortical bone (n = 3; p = 0.00771), and also in trabecular bone (n = 3; p = 0.00014). The transverse section of femoral bone exhibits higher longitudinal elastic moduli compared to the transverse elastic moduli in the longitudinal section. The anisotropy ratio in our tests varies from 1.2–2.

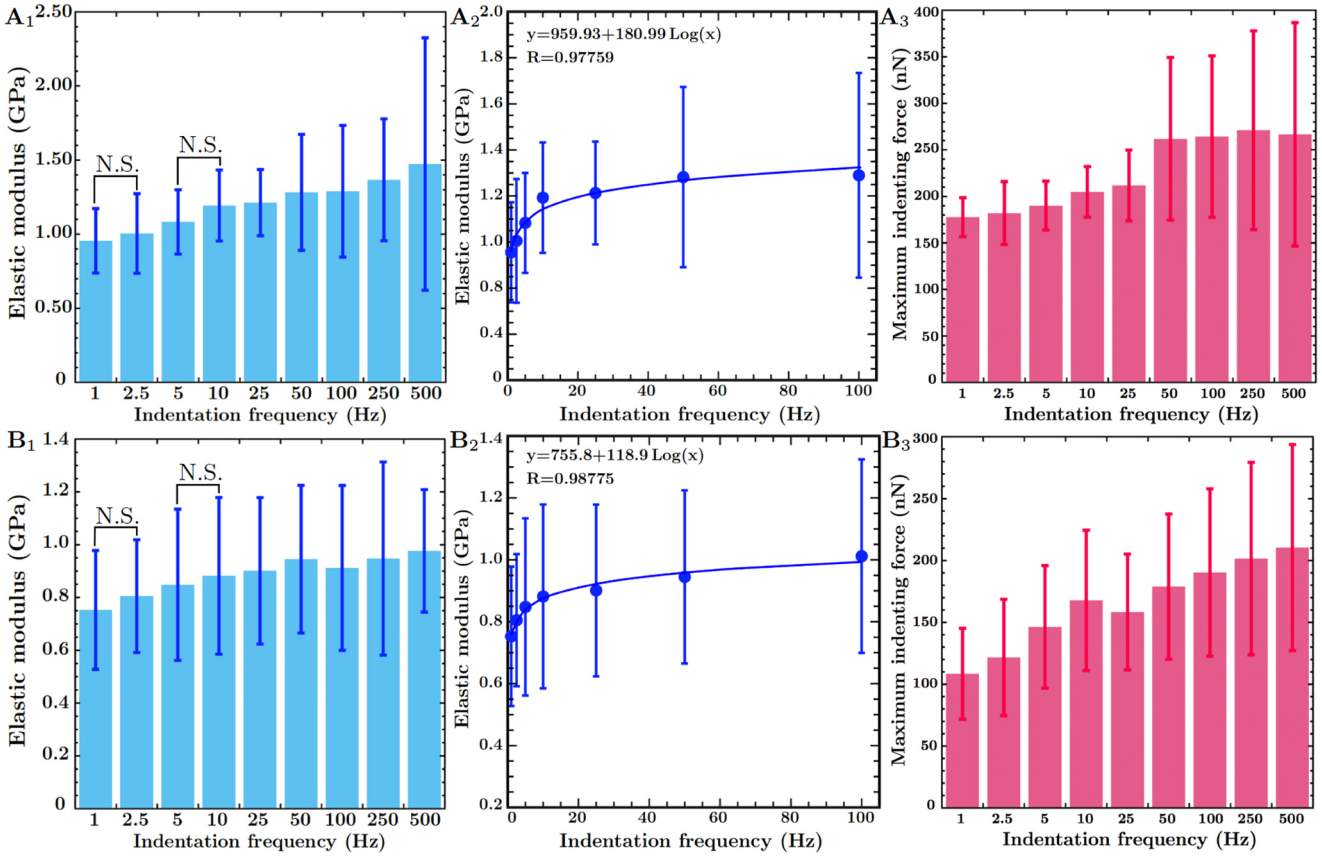

Fig. 9. A_1: Longitudinal elastic modulus E_l of cortical bone at values of indentation frequency $[1/(T_e + T_r)]$ from 1 to 500 Hz. The mean value of E_l increased from ~ 1.5 GPa at 1 Hz to ~ 2.2 GPa at 500 Hz (statistically significant difference with p = 0.0008). A_2: E_l of cortical bone at 1–100 Hz plotted with a logarithmic fit. B_1: Longitudinal elastic modulus E_l of trabecular bone at values of indentation frequency from 1–500 Hz. The mean value of E_l increased from ~ 0.75 GPa at 1 Hz to ~ 1 GPa at 500 Hz (statistically significant difference with p = 0.0017). B_2: E_l of trabecular bone at 1–100 Hz plotted with a logarithmic fit. Force maps containing 32 × 32, 64 × 64, or 128 × 128 indentation points were created on each sample. The elastic moduli of cortical and trabecular bone at higher frequencies are greater than those at lower frequencies; A_3 & B_3: Maximum indenting force in cortical and trabecular bone. For a given indentation depth, δ, (i.e., smaller than 50 nm), the indenting force, F, increases as the loading rate increases, showing the dependence of the stiffness of the bone surface to the loading rate. The structure of cortical and trabecular bone changes throughout the bone, which is indicative of its inhomogeneity. N.S. represents no significant difference (p > 0.05).

age, sex, and other non-structural factors such as the mouse strain, which depends on its genetic make-up.

The heterogeneous variation of the elastic moduli reported in the literature for both human and bovine femora (Nobakhti et al., 2017; Wirtz et al., 2000) highlights the relations between structure and material properties of bone tissue. Our results attest the existence of elasticity gradients as shown in Table 1, where the elastic measures vary with position. In particular, from the middle third and the posterior quadrant of the femur, the largest mean value of the elastic modulus was measured in the axial direction (~ 1.8–2 GPa), whereas the lowest value appeared in the distal third and anterior quadrant of the femur (~ 0.8–1 GPa). The elastic modulus of cortical bone at the distal and proximal ends of the femur is lower (≈ 30%) than that at the diaphyseal portion (~ 1.2–1.5 GPa). The elastic modulus decreases from the femur head, where the femur connects to the pelvic bone at the acetabulum, to the distal part, where the femur articulates with the tibia at the knee. In these regions of transition from hard bone to the soft connective tissues, e.g. ligaments and cartilage, the value of the elastic modulus is ~ 0.5 GPa. The existence of elasticity gradients observed here for the mouse femur parallels the findings of previous experimental and numerical work on human and bovine femoral bone (Nobakhti et al., 2017; Wirtz et al., 2000).

We note that the values reported above for the elastic moduli strongly depend on the Poisson's ratio, ν, assumed for the bone tissue. From previous studies (Reilly et al., 1974; Sharir et al., 2008; Wirtz et al., 2000), ν typically ranged from 0.2–0.4, and within these limits, the elastic modulus was shown to vary less than 8% (Rho et al., 1997). In our study accounting for multiple bone samples and orientations, the Poisson's ratio was also assumed in the range 0.2–0.45, within which the difference in elastic modulus was ~ 18.2% for cortical bone, and ≈ 19.5% for trabecular bone (Fig. 5).

Nanoindentation and classical macroscopic testing, such as bending and tensile tests, are inherently different technologies because they provide measures of material properties at dissimilar length scales. The distinction between the two is caused by the volume of material each of them can handle: the former examines nanoscale surface features, whereas the latter shaped specimen with specific geometry (Hengsberger et al., 2003). Disparity therefore can be observed in the values of the elastic modulus they can measure. Macroscopic characterization provides bulk properties that account for the contribution of the whole sample geometry as well as its porosity, whereas nanoindentation analysis gauges the local properties of the specimen, obtained from the interaction between the AFM spherical tip and the sample surface. In addition, the strains applied during nanoindentation are typically much smaller (about 2 orders of magnitude lower) than the strain used in macroscopic tests. The values reported in this work cannot thus be compared with those obtained through macroscopic tests (Schriefer et al., 2005).

4.2. Bone viscoelasticity via AFM

Bone viscoelasticity arises from the water content of the tissue and

proteoglycans. Previous works showed a similarity in the shape of the relaxation curves obtained for normal and demineralized bones (Sasaki et al., 1993; Garner et al., 2000). Our results show a correlation between loading frequency and elastic modulus for both trabecular and cortical bone. For prescribed indentation depth, the maximum indentation load increased with the loading frequency, thereby confirming high values of elastic modulus at high loading frequencies, as typically observed in biological samples (Asgari et al., 2017; Asgari, 2017). For cortical bone, the mean value of the longitudinal elastic modulus increased from ~ 1.5 GPa at 1 Hz to ~ 2.2 GPa at 500 Hz, showing more than 40% increase. For trabecular bone, the increase was about 30% from ~ 0.75 GPa at 1 Hz, to ~ 1 GPa at 500 Hz (Fig. 9). This variation can be attributed to the proteinaceous nature of collagen fibrils at the molecular scale (Asgari et al., 2017), and the direct correlation between elastic modulus and frequency is a result of the viscoelastic nature of bone (Garner et al., 2000).

For each sample of the cortical and trabecular bone tissues, we established through a logarithmic fit the correlation between the longitudinal elastic modulus E_l and the indentation frequency (Fig. 9A_2 and B_2). The data include seven frequency points below 100 Hz, and only two frequencies above that value (250 Hz, and 500 Hz). To obtain the best fit, the frequency domain was between 1 and 100 Hz. Our correlation between the elastic modulus and the loading frequency resembles that of other biological samples such as collagen type I and III (Asgari et al., 2017), thus confirming the viscoelastic nature of our bone tissue samples.

Earlier studies on wet and dry bovine femoral bone tissues via nanoindentation showed the influence of water content in their elastic and strength properties (Rho et al., 1993; Rho and Pharr, 1999; Zysset et al., 1999; Schwiedrzik et al., 2017; Hengsberger et al., 2002). For wet bone, the elastic modulus of the interstitial lamellae was reported ~ 15% higher than that of the osteons, while for dry bone this value was ~ 10% (Rho and Pharr, 1999). Other studies also examined the role of dehydration on the elastic response of cortical and trabecular bone at given anatomical sites. For the former, the elastic modulus was shown to increase up to 9–15% with the degree of dehydration, and be larger in the interstitial rather than in the osteonal bone (Rho et al., 1993; Rho and Pharr, 1999; Zysset et al., 1999). For the latter, lower values were reported (Rho et al., 1993; Rho and Pharr, 1999; Zysset et al., 1999; Hengsberger et al., 2002). The results of our study show that sample dehydration causes up to ~ 22% increase in the longitudinal elastic modulus and up to ~ 27.5% increase in the transverse elastic modulus. This change can be attributed to the presence of fluid in the extracellular matrix of the tissue, a factor that reduces the mechanical properties of the bone tissue (Asgari et al., 2017). On the other hand, dehydration of samples of collagen fibrils increases their elastic modulus above the values obtained for samples immersed in Phosphate-buffered saline, a result consistent with previous studies (Buehler, 2006; Grant et al., 2008; Asgari et al., 2017; Latifi et al., 2018).

The choice of the mouse age in this study stems from previous findings (Ferguson et al., 2003), which investigated the age-related effect on bone development in mice. Therein a rapid bone growth was reported for young mice, marked by substantial increases in bone size, mineral mass, and changes in material properties. Skeletal maturity was achieved between 12 and 42 weeks of age, after which a maintenance of bone mass and mechanical properties was observed. Given this work examines the nanomechanics of the mouse femur at skeletal maturity, we focus on adult mice of given age and sex at a static stage in development, as opposed to a dynamic state of growth.

In summary, in this work, we used AFM-indentation to conduct a systematic investigation on the elasticity of femoral bone tissue of the adult mouse. For both trabecular and cortical bone, the morphological characteristics have been unveiled with an emphasis on the bone microstructures, and their nanoscale properties have been measured locally in distinct directions along and across the femur. The comprehensive set of data gathered here on the elastic properties can serve as a foundation for further work on all fronts of bone research including experimental, numerical, and theoretical studies. For instance, a follow-up nanoscale investigation can serve to appraise the role of mouse-specific factors, such as age and gene knockout, on the nano scale elastic properties of the mouse bone tissue. Our results could also be further used to develop phenomenological as well as numerical models that relate the elastic moduli of bone tissue to its mineral density, hence providing a more comprehensive assessment of the multiscale properties of bone tissues at large.

5. Conclusion

This work provided a quantitative analysis of the elastic behavior of bone tissues in the adult mouse femur. Atomic Force Microscopy (AFM) indentation was used to characterize the elasticity of cortical and trabecular bone of mouse femora, and to assess the degree of inhomogeneity and anisotropy in both longitudinal and transverse directions. In the longitudinal direction, $\sim 1.98 \pm 0.62$ GPa was the largest value of the elastic modulus measured for cortical bone. Other differences in elastic modulus could be attributed to the bone type and measurement direction. For cortical bone, the elastic modulus was ≈ 15% higher in the longitudinal than in the transverse direction. For trabecular bone, lower ranges ($\sim 0.92 \pm 0.22$ GPa) appeared in the longitudinal direction. In the transverse direction, the values of $\sim 1.58 \pm 0.36$ GPa and $\sim 0.55 \pm 0.21$ GPa were obtained for the elastic moduli of cortical and trabecular bone, respectively. In the distal regions, a 70% reduction was observed for the average transverse elastic modulus of cortical bone. Furthermore, for cortical bone, a significant variation in the longitudinal elastic modulus appeared along the femur only, as opposed to across the femur. A correlation was also established between indentation frequency and elastic modulus for both types of bone tissue. For cortical bone, an increase of 45% was observed for the mean value of the longitudinal elastic modulus, from 1.5 GPa at 1 Hz to 2.2 GPa at 500 Hz. For trabecular bone, a moderate increase of ≈ 30% was measured from 0.75 GPa at 1 Hz to 1 GPa at 500 Hz.

CRediT authorship contribution statement

Meisam Asgari: Conceptualization, Methodology, Formal analysis, Writing - original draft, Writing - review & editing. **Jad Abi-Rafeh:** Data curation, Writing - review & editing. **Geoffrey N. Hendy:** Data curation, Writing - review & editing. **Damiano Pasini:** Conceptualization, Methodology, Formal analysis, Writing - original draft, Writing - review & editing.

Acknowledgements

M.A. gratefully acknowledges Dr. Natalie Reznikov at McGill's Faculty of Dentistry, and Cassidy R. Vanderschee at McGill's Department of Chemistry for fruitful discussions. D.P. acknowledges support from the Natural Sciences and Engineering Research Council of Canada (NSERC), the Canadian Institutes of Health Research (CIHR), and the Canadian Foundation for Innovation (CFI grant 229251). G.N.H. acknowledges support from the CIHR (MOP-142269). J. A-R. acknowledges awards from CIHR, Endocrine Society, American Society for Bone and Mineral Research, and RSBO.

Appendix A. Supplementary data

Supplementary data associated with this article can be found in the online version at doi:10.1016/j.jmbbm.2019.01.024.

References

Martin, D.E., Severns, A.E., Kabo, J.M., 2004. Determination of mechanical stiffness of bone by pQCT measurements: correlation with non-destructive mechanical four-point

bending test data. J. Biomech. 37 (8), 1289–1293.
Olszta, M.J., Cheng, X., Jee, S.S., Kumar, R., Kim, Y.-Y., Kaufman, M.J., Douglas, E.P., Gower, L.B., 2007. Bone structure and formation: a new perspective. Mater. Sci. Eng. R Rep 58, 77–116.
Hamed, E., Jasiuk, I., 2012. Elastic modeling of bone at nanostructural level. Mater. Sci. Eng. R Rep 73 (3), 27–49.
Lees, S., 1987. Considerations regarding the structure of the mammalian mineralized osteoid from viewpoint of the generalized packing model. Connect. Tissue Res. 16, 281–303.
Garner, E., Lakes, R., Lee, T., Swan, C., Brand, R., 2000. Viscoelastic dissipation in compact bone: implications for stress-induced fluid flow in bone. J. Biomech. Eng. 122, 166–172.
Hamed, E., Lee, Y., Jasiuk, I., 2010. Multiscale modeling of elastic properties of cortical bone. Acta Mech. 213, 131–154.
Depalle, B., Qin, Z., Shefelbine, S.J., Buehler, M.J., 2016. Large deformation mechanisms, plasticity, and failure of an individual collagen fibril with different mineral content. J. Bone Miner. Res. 31 (2), 380–390.
Fratzl, P., Gupta, H.S., Paschalis, E.P., Roschger, P., 2004. Structure and mechanical quality of the collagen-mineral nano-composite in bone. J. Mater. Chem. 14, 2115–2123.
Fratzl, P., 2008. Collagen: Structure and Mechanics. Springer, New York.
Buehler, M.J., 2006. Nature designs tough collagen: explaining the nanostructure of collagen fibrils. Proc. Natl. Acad. Sci. USA 103, 12285–12290.
Buehler, M.J., 2007. Molecular nanomechanics of nascent bone: fibrillar toughening by mineralization. Nanotechnology 18, 295102.
Sharir, A., Barak, M.M., Shahar, R., 2008. Whole bone mechanics and mechanical testing. Vet. J. 177, 8–17.
Turner, C.H., Burr, D.B., 1993. Basic biomechanical measurements of bone: a tutorial. Bone 14 (4), 595–608.
Rho, J.Y., Kuhn-Spearing, L., Zioupos, P., 1998. Mechanical properties and the hierarchical structure of bone. Med. Eng. Phys. 20 (2), 92–102.
Hofmann, T., Heyroth, F., Meinhard, H., Fränzel, W., Raum, K., 2006. Assessment of composition and anisotropic elastic properties of secondary osteon lamellae. J. Biomech. 39 (12), 2282–2294.
Weiner, S., Wagner, H.D., 1998. The material bone: structure-mechanical function relations. Annu. Rev. Mater. Sci. 28 (1), 271–298.
Gibson, L., 1985. The mechanical behavior of cancellous bone. J. Biomech. 18 (5), 317–328.
Cowin, S.C., 2001. Bone Mechanics Handbook. CRC Press, Taylor Francis Group, Florida.
Currey, J.D., 2002. Bones: Structure and Mechanics. Princeton University Press, Princeton, NJ.
Carter, D.R., Beaupre, G.S., 2007. Skeletal Function and Form: Mechanobiology of Skeletal Development, Aging, and Regeneration. Cambridge University Press, Cambridge, UK.
Ashman, R.B., Rho, J.Y., 1988. Elastic modulus of trabecular bone material. J. Biomech. 21 (3), 177–181.
Rho, J.Y., Tsui, T.Y., Pharr, G.M., 1997. Elastic properties of human cortical and trabecular lamellar bone measured by nanoindentation. Biomaterials 18, 1325–1330.
Weiner, S., Traub, W., Wagner, H.D., 1999. Lamellar bone: structure-function relations. J. Struct. Biol. 126, 241–255.
Reznikov, N., Shahar, R., Weiner, S., 2014. Bone hierarchical structure in three dimensions. Acta Biomater. 10, 3815–3826.
Choi, K., Goldstein, S.A., 1992. A comparison of the fatigue behavior of human trabecular and cortical bone tissue. J. Biomech. 25 (12), 1371–1381.
Reznikov, N., Chase, H., Brumfeld, V., Shahar, R., Weiner, S., 2015. The 3D structure of the collagen fibril network in human trabecular bone: relation to trabecular organization. Bone 71, 189–195.
Keaveny, T.M., Morgan, E.F., Niebur, G.L., Yeh, O.C., 2001. Biomechanics of trabecular bone. Annu. Rev. Biomed. Eng. 3, 307–333.
McKee, M.D., Nanci, A., 1996. Osteopontin at mineralized tissue interfaces in bone, teeth, and osseointegrated implants: ultrastructural distribution and implications for mineralized tissue formation, turnover, and repair. Microsc. Res. Tech. 33 (2), 141–164.
Zysset, P.K., Guo, X.E., Hoffler, C.E., Moore, K.E., Goldstein, S.A., 1999. Elastic modulus and hardness of cortical and trabecular bone lamellae measured by nanoindentation in the human femur. J. Biomech. 32, 1005–1012.
Donnelly, E., 2011. Methods for assessing bone quality: a review. Clin. Orthop. Relat. Res. 469, 2128–2138.
Townsend, P.R., Rose, R.M., Radin, E.L., 1975. Buckling studies of single human trabeculae. J. Biomech. 8 (3), IN5–IN6.
Ryan, S.D., Williams, J.L., 1989. Tensile testing of rodlike trabeculae excised from bovine femoral bone. J. Biomech. 22 (4), 351–355.
Bayraktar, H.H., Morgan, E.F., Niebur, G.L., Morris, G.E., Wong, E.K., Keaveny, T.M., 2004. Comparison of the elastic and yield properties of human femoral trabecular and cortical bone tissue. J. Biomech. 37 (1), 27–35.
Beaupied, H., Lespessailles, E., Benhamou, C., 2007. Evaluation of macrostructural bone biomechanics. Joint Bone Spine 74 (3), 233–239.
Woo, S.L.-Y., Hollis, J.M., Adams, D.J., Lyon, R.M., Takai, S., 1991. Tensile properties of the human femur-anterior cruciate ligament-tibia complex: the effects of specimen age and orientation. Am. J. Sports Med. 19 (3), 217–225.
Bala, Y., Farlay, D., Boivin, G., 2013. Bone mineralization: from tissue to crystal in normal and pathological contexts. Osteoporos. Int. 24, 2153–2166.
Eriksen, E.F., Axelrod, D.W., Melsen, F., 1994. Bone Histomorphometry. Raven Press.
Hengsberger, S., Kulik, A., Zysset, P.H., 2002. Nanoindentation discriminates the elastic properties of individual human bone lamellae under dry and physiological conditions. Bone 30, 178–184.
Katz, J.L., Meunier, A., 1993. Scanning acoustic microscope studies of the elastic properties of osteons and osteon lamellae. J. Biomech. Eng. 115, 543–548.
Fan, Z., Smith, P.A., Eckstein, E.C., Harris, G.F., 2006. Mechanical properties of OI type III bone tissue measured by nanoindentation. J. Biomed. Mater. Res. 79, 71–77.
Turner, C.H., Rho, J.Y., Takano, Y., Tsui, T.Y., Pharr, G.M., 1999. The elastic properties of trabecular and cortical bone tissues are similar: results from two microscopic measurement techniques. J. Biomech. 32 (4), 437–441.
Rho, J.Y., Ashman, R.B., Turner, C.H., 1993. Young's modulus of trabecular and cortical bone material: ultrasonic and microtensile measurements. J. Biomech. 26, 111–119.
Rho, J.Y., Zioupos, P., Currey, J.D., Pharr, G.M., 1999. Variations in the individual thick lamellar properties within osteons by nanoindentation. Bone 25 (3), 295–300.
Rho, J.Y., Pharr, G.M., 1999. Effects of drying on the mechanical properties of bovine femur measured by nanoindentation. J. Mater. Sci. Mater. Med 10, 485–488.
Thurner, P.J., 2009. Atomic force microscopy and indentation force measurement of bone. Nanomed. Nanobiotechnol 1 (6), 624–649.
Donnelly, E., Baker, S.P., Boskey, A.L., van der Meulen, M.C.H., 2006. Effects of surface roughness and maximum load on the mechanical properties of cancellous bone measured by nanoindentation. J. Biomed. Mater. Res. A 77, 426–435.
Katsamenis, O.L., Jenkins, T., Thurner, P.J., 2015. Toughness and damage susceptibility in human cortical bone is proportional to mechanical inhomogeneity at the osteonal-level. Bone 76, 158–168.
Hansma, P.K., Turner, P.J., Fantner, G.E., 2006. Bone diagnostic instrument. Rev. Sci. Instrum 77, 075105.
Setters, A., Jasiuk, I., 2014. Towards a standardized reference point indentation testing procedure. J. Mech. Behav. Biomed. Mater 34, 57–65.
Idkaidek, A., Agarwal, V., Jasiuk, I., 2017. Finite element simulation of Reference Point Indentation on bone. J. Mech. Behav. Biomed. Mater. 65, 574–583.
Hassenkam, T., Fantner, G.E., Cutroni, J.A., Weaver, J.C., Morse, D.E., Hansma, P.K., 2004. High-resolution AFM imaging of intact and fractured trabecular bone. Bone 35, 4–10.
Wallace, J.M., 2012. Applications of atomic force microscopy for the assessment of nanoscale morphological and mechanical properties of bone. Bone 50 (1), 420–427.
Crabtree, J.S., Scacheri, P.C., Ward, J.M., Garrett-Beal, L., Emmert-Buck, M.R., Edgemon, K.A., Lorang, D., Libutti, S.K., Chandrasekharappa, S.C., Marx, S.J., Spiegel, A.M., Collins, F.S., 2001. A mouse model of multiple endocrine neoplasia, type 1, develops multiple endocrine tumors. Proc. Natl. Acad. Sci. U.S.A 98, 1118–1123.
Kanazawa, I., Canaff, L., Rafeh, J.A., Angrula, A., Li, J., Riddle, R.C., Boraschi-Diaz, I., Komarova, S.V., Clemens, T.L., Murshed, M., Hendy, G.N., 2015. Osteoblast menin regulates bone mass in vivo. J. Biol. Chem. 290, 3910–3924.
Xu, J., Rho, J.Y., Mishra, S.R., Fan, Z., 2003. Atomic force microscopy and nanoindentation characterization of human lamellar bone prepared by microtome sectioning and mechanical polishing technique. J. Biomed. Mater. Res. Part A 67 (3), 719–726.
Hansma, P.K., Fantner, G.E., Kindt, J.H., Thurner, P.J., Schitter, G., Turner, P.J., Udwin, S.F., Finch, M.M., 2005. Sacrificial bonds in the interfibrillar matrix of bone. J. Musculoskelet. Neuronal Interact 5, 313.
Wirtz, D.C., Schiffers, N., Pandorf, T., Radermacher, K., Weichert, D., Forst, R., 2000. Critical evaluation of known bone material properties to realize anisotropic FE-simulation of the proximal femur. J. Biomech 33, 1325–1330.
Nobakhti, S., Katsamenis, O., Zaarour, N., Limbert, G., Thurner, P.J., 2017. Elastic modulus varies along the bovine femur. J. Mech. Behav. Biomed. Mater 71, 279–285.
Reilly, D.T., Burstein, A.H., Frankel, V.H., 1974. The elastic modulus for bone. J. Biomech 7 (3) 271IN9273–272IN12275.
Asgari, M., 2017. Micro-mechanical, continuum-mechanical, and AFM-based descriptions of elasticity in open cylindrical micellar filaments. Soft Matter 13, 7112–7128.
Swadener, J.G., Rho, J.Y., Pharr, G.M., 2001. Effects of anisotropy on elastic moduli measured by nanoindentation in human tibial cortical bone. J. Biomed. Mater. Res. Part A 57 (1), 108–112.
Swadener, J.G., Pharr, G.M., 2001. Indentation of elastically anisotropic half-spaces by cones and parabolae of revolution. Philos. Mag. A 81 (2), 447–466.
Eppell, S.J., Tong, W., Katz, J.L., Kuhn, L., Glimcher, M.J., 2001. Shape and size of isolated bone mineralites measured using atomic force microscopy. J. Orthop. Res. 19, 1027–1034.
Thurner, P.J., Oroudjev, E., Jungmann, R., Kreutz, C., Kindt, J.H., Schitter, G., Okouneva, T.O., Lauer, M.E., Fantner, G.E., Hansma, H.G., 2007. Imaging of bone ultrastructure using atomic force microscopy. Modern Research and Educational Topics in Microscopy 37–48.
Thompson, J.B., Kindt, J.H., Drake, B., Hansma, H.G., Morse, D.E., Hansma, P.K., 2001. Bone indentation recovery time correlates with bond reforming time. Nature 414, 773.
Kindt, J.H., Fantner, G.E., Thurner, P.J., Schitter, G., Hansma, P.K., 2005. A new technique for imaging mineralized fibrils on bovine trabecular bone fracture surfaces by atomic force microscopy. Mater. Res. Soc. Symp. Proc. 874, 12.1–12.7.
Rho, J.Y., Roy, M.E., Tsui, T.Y., Pharr, G.M., 1999. Elastic properties of microstructural components of human bone tissue as measured by nanoindentation. J. Biomed. Mater. Res. Part A 45, 48–54.
Choi, K., Kuhn, J.L., Ciarelli, M.J., Goldstein, S.A., 1990. The elastic moduli of human subchondral, trabecular, and cortical bone tissue and the size-dependency of cortical bone modulus. J. Biomech 23 (11), 1103–1113.
Martin, R.B., 1991. Determinants of the mechanical properties of bones. J. Biomech 24, 79–88.
Manilay, Z., Novitskaya, E., Sadovnikov, E., McKittrick, J., 2013. A comparative study of young and mature bovine cortical bone. Acta Biomater 9, 5280–5288.
Hengsberger, S., Enstroem, J., Peyrin, F., Zysset, P.H., 2003. How is the indentation modulus of bone tissue related to its macroscopic elastic response? A validation study. J. Biomech 36, 1503–1509.
Schriefer, J.L., Robling, A.G., Warden, S.J., Fournier, A.J., Mason, J.J., Turner, C.H.,

2005. A comparison of mechanical properties derived from multiple skeletal sites in mice. J. Biomech 38 (3), 467–475.
Sasaki, N., Nakayama, Y., Yoshikawa, M., Enyo, A., 1993. Stress relaxation function of bone and bone collagen. J. Biomech 26, 1369–1376.
Asgari, M., Latifi, N., Heris, H.K., Vali, H., Mongeau, L., 2017. In vitro fibrillogenesis of tropocollagen type III in collagen type I affects its relative fibrillar topology and mechanics. Sci. Rep. 7 (1), 1392.
Schwiedrzik, J., Taylor, A., Casari, D., Wolfram, U., Zysset, P., Michler, J., 2017. Nanoscale deformation mechanisms and yield properties of hydrated bone extracellular matrix. Acta Biomater 60, 302–314.
Latifi, N., Asgari, M., Vali, H., Mongeau, L., 2018. A tissue-mimetic nano-fibrillar hybrid injectable hydrogel for potential soft tissue engineering applications. Sci. Rep. 8 (1), 1047.
Grant, C.A., Brockwell, D.J., Radford, S.E., Thomson, N.H., 2008. Effects of hydration on the mechanical response of individual collagen fibrils. Appl. Phys. Lett. 92, 233902.
Ferguson, V.L., Ayers, R.A., Bateman, T.A., Simske, S.J., 2003. Bone development and age-related bone loss in male C57BL/6J mice. Bone 33 (3), 387–398.